Optical Absorption and Electron-Energy-Loss Spectra of Helium Microbubbles in Aluminum

J. C. Rife
Optical Probes Branch, Naval Research Laboratory, Washington, D. C. 20375

and

S. E. Donnelly, A. A. Lucas, and J. M. Gilles
Institute for Research in Interface Sciences, Facultés Universitaires Notre Dame de la Paix, B-5000 Namur, Belgium

and

J. J. Ritsko
Xerox Webster Research Center, Webster, New York 14580
(Received 28 January 1981)

Aluminum thin films containing helium microbubbles produced by He^+-ion implantation have been investigated by ultraviolet absorption and electron-energy-loss spectroscopies in the range 1–30 eV. The shape and position of the 1^1S_0-n^1P_1 helium line series and several Al plasmon bands are discussed in terms of the physical state of helium in the bubbles. Results imply helium densities 3 to 6 times that of liquid He at 2°K and 1 bar pressure.

PACS numbers: 78.40.Kc, 33.20.Lg, 61.70.Tm, 71.45.Gm

Because of its strongly repulsive pseudopotential, helium has a negative heat of solution in metals[1] and tends to cluster with vacancies to form bubbles of extremely high gas density. These bubbles range from tens to hundreds of angstroms in diameter. At sufficient doses and for certain implantation profiles, helium bubbles induce blistering, flaking, and erosion of an implanted metal surface.[2-4] These damage phenomena, which are not fully understood, pose potential problems for fusion reactors by contaminating the plasma with high-Z impurities and possibly by decreasing wall lifetime.

Up to now, experimental probes of helium bubbles have been primarily limited to transmission electron microscopy (TEM). In order to investigate the physical state of helium, we intended to measure the pressure shift and broadening of the helium 1^1S_0-2^1P_1 resonance line. Such an approach was encouraged by the calculation of Ohtaka and Lucas[5] which indicated that line-broadening mechanisms in the helium-aluminum system other than pressure broadening should be negligible for bubbles larger than 20 Å in diameter.

Specimen preparation has been discussed in greater detail elsewhere.[6] The specimen substrates were $\simeq 2000$-Å-thick Al thin films mounted on 3-mm-diam Cu TEM grids with an aperture of 0.6 mm. The specimens were bombarded at room temperature with 5-keV helium ions. Helium content was determined by resonance proton backscattering. At 5 keV, the helium penetration depth is $\simeq 750$ Å with a straggling of $\simeq 350$ Å, and local helium concentration could be up to 3 times what average concentration measurements indicate. Bubble size distributions in our specimens were monitored by TEM. The smallest bubble size resolved was $\simeq 20$ Å in diameter.

Ultraviolet absorption measurements were made on the 2.2-m grazing incidence monochromator at the National Bureau of Standards Synchrotron Ultraviolet Radiation Facility (SURF) synchrotron radiation source. The apparatus and some preliminary measurements have been discussed previously.[6,7] Ultraviolet spot size on sample was $<2\times 2$ mm^2, and energy resolution was $\simeq 0.07$ eV.

Electron-energy-loss measurements were performed at the Xerox Webster Research Center with an 80-keV electron beam. Beam currents were $\simeq 10^{-8}$ A over a 1-mm^2 spot size. Resolution was 0.1 eV with momentum transfer less than 0.03 Å^{-1}.

Optical absorption and electron-energy-loss spectroscopy (EELS) data near 21.2 eV for a 1.45-at.%-He and a 3.1-at.%-He specimen are shown in Figs. 1 and 2, respectively. The absorption data are plotted as the optical density of noncharacteristic aluminum absorption, i.e., the logarithm of the ratio of fluxes through nonbombarded and bombarded films. A background due to enhanced oxygen content in the implanted specimen has been subtracted away. The EELS data plot the loss junction, $\alpha - \mathrm{Im}(1/\epsilon)$, with a constant background equal to about two-thirds the peak

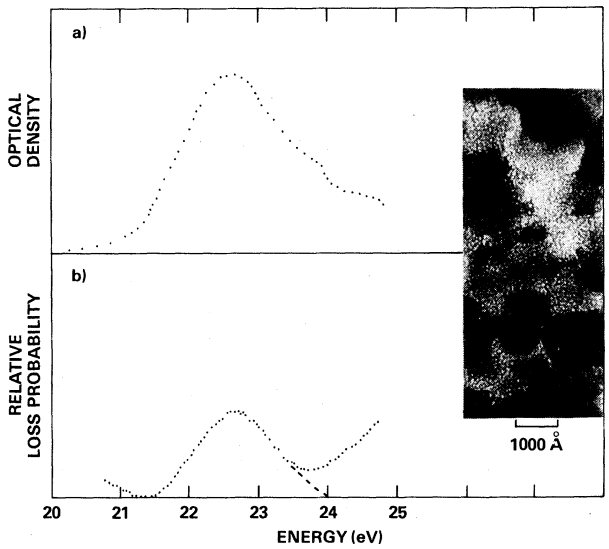

FIG. 1. 1.45 at.% He in Al. (a) Relative absorption spectrum (peak optical density is $\simeq 0.8$). (b) Electron-energy-loss spectrum (dashed line above 23 eV shows loss with multiple scattering removed). Inset: transmission electron micrograph.

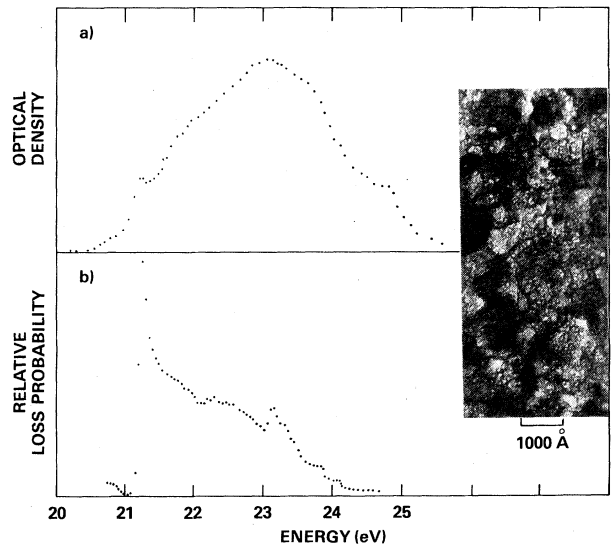

FIG. 2. 3.1 at.% He in Al. (a) Relative absorption spectrum (peak optical density is $\simeq 1.1$). (b) Electron-energy-loss spectrum. Inset: transmission electron micrograph.

count rate subtracted away. The flat EELS background is due to multiple scattering including cavity surface plasmon losses. The relative EELS magnitudes in Figs. 1 and 2 are correct since the spectra have been normalized to their respective bulk plasmon losses.

In Fig. 1, the TEM micrograph shows a sharply peaked bubble size distribution for the 1.45-at.% specimen with bubbles 50 ± 10 Å in diameter. The peaks at 22.6 in Figs. 1(a) and 1(b) can be identified as the helium resonance line shifted 1.4 eV to higher energies and broadened to at least 1.2 eV [full width at half maximum (FWHM)]. Our interpretation of the results is an inhomogeneous broadening and shift to the blue of the He 1^1S_0-2^1P_1 transition due to "Pauli exclusion" of the excited $2p$ orbital by the filled $1s$ shells of neighboring ground-state atoms. This interpretation is inspired by the argument of Surko *et al.*,[8] who invoked the weakly repulsive $^1\Pi_u$ state of the He_2 excimer at large nuclear separation to explain the 0.2-eV blue shift of the helium resonance line in the reflectance of liquid helium. Potential energy curves for the $^1\Pi_u$ and $^1\Sigma_u^+$ states of $2p$ character in He_2 are given by Browne[9] and by Guberman and Goddard,[10] respectively.

For a dense fluid we need a statistical average of the potential energy of an excited atom in its repulsive coordination with normal atoms. In first-order perturbation theory, this is

$$\Delta_{2P} = \langle \sum \langle 2p | V(\vec{r} - \vec{R}_i) | 2p \rangle \rangle_{\text{av}}, \tag{1}$$

where V is the (pseudo) potential of the filled $1s^2$ shell of the atom at position $\vec{R}_i$ for the $2p$ electron on the central atom. We are performing pseudopotential calculations along the lines developed by Jortner *et al.*[11] for electrons in liquid He and the details will appear elsewhere. For our present purpose of a semiquantitative evaluation, we will use a simple model consisting of δ-function repulsive cores for the ground-state He atoms. As noted by Guberman and Goddard,[10] this provides a valid approximation to their accurate result for the He_2 dimer as long as the nuclear separation $\vec{R}_i$ exceeds 2 Å. The $2P$ level shift in the fluid is then given by

$$\Delta_{2P} = nC(\alpha^5/24) \int_0^\infty dR\, R^4 g(R) \exp(-\alpha R), \tag{2}$$

where $\alpha = 1.83$ Å^{-1} is twice the $2p$ orbital exponent, n is the He fluid density, $g(R)$ is its radial distribution function, and C is the strength of the δ-function pseudopotential. By fitting the large-R tail of the $^1\Sigma_u^+$ dimer potential curve,[10] a theoretical value of $C_{\text{th}} \simeq 40$ eV Å^3 obtains, whereas using the measured[12] low-temperature liquid $g(R)$ in (2) along with $\Delta_{2P}(\text{liquid}) = 0.2$ eV (Ref. 8) gives an experimental value of $C_{\text{ex}} = 20$ eV Å^3 only. As for the room-temperature He gas in the bubbles, we do not know its accurate $g(R)$ but we can approximate it by a unit step function[13] at $R = \sigma$

$\simeq 2.556$ Å, the He Lennard-Jones radius.

One then obtains from (1) $\Delta_{2P} = 0.5nC$ and our observed 1.4-eV blue shift implies a He density of $(7-14)\times 10^{22}$ cm^{-3}, depending on whether C_{th} or C_{ex} is trusted. Such densities should be compared with the Al density of 6×10^{22} cm^{-3} and with the He hard-sphere maximum packing of $\sqrt{2}/\sigma^3 \sim 8.5\times 10^{22}$ cm^{-3}. Hence, on the basis of this simple model and of our spectroscopic measurements, He densities in small bubbles are predicted to lie in the range of one to two atoms per Al vacancy. Such packing is consistent with the measured He average content, bubble density, and diameter in the 1.45-at.% specimen if we assume no significant amount of submicroscopically trapped He. As to the pressure in the bubbles, at these densities compressibility results[14] for helium at 298 K imply pressures above 10^4 bars, i.e., in excess of the equilibrium value $4\gamma/d \approx 8000$ bars given by the pressure of the bubble surface tension γ. A more precise determination of density and pressure will require refinement of the theory and will be of great value in understanding the mechanisms of bubble formation and growth.

Turning to the spectra of Fig. 2, notable differences appear between the optical absorption and EELS data for the 3.1-at.% specimen. The TEM micrograph shows a bubble size distribution with many bubbles around 20 Å in diameter tailing off to fewer larger ones up to 200 Å in diameter, so that with equilibrium pressures one might expect about the same number of helium atoms in large bubbles as in small ones. One would expect an absorption spectrum with very little broadening and shift for the lowest-pressure, big cavities, and one with large blue shifts and broadening for the large number of very small bubbles. Indeed, the optical absorption now exhibits a reproducible structure consisting of a weak and narrow peak close to 21.2 eV superimposed as a shoulder on a peak somewhat broader (2.2 eV, FWHM) than that of Fig. 1, but similarly displaced by 2 eV towards shorter wavelengths. In the EELS spectrum of Fig. 2(b), the sharper feature corresponding to the resonance line at 21.2 eV is prominent over the broad peak extending between 21 and 25 eV. In addition, the EELS spectrum reveals a series of three further narrow peaks at 23.11, 23.81, and 24.06 eV whose positions and intensities are consistent with the transitions 1^1S_0-n^1P_1, $n = 3, 4, 5$.[15] This implies that a substantial fraction of He in this specimen must be contained in larger bubbles at pressures sufficiently reduced for the He atoms to exhibit more fully their discrete atomic spectrum.

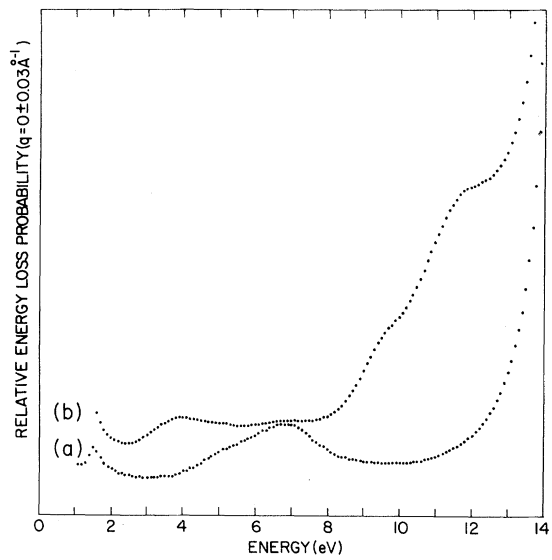

FIG. 3. Electron-energy-loss spectra below 15 eV of curve *a*, nonbombarded Al film, and curve *b*, 1.45 at.% He in Al. The Al bulk plasmon peak heights have been matched at 15 eV.

We attribute the better EELS resolution for atomic features to specimen transverse inhomogeneity. We contend that the films are locally thinner above large bubbles because the implantation-induced swelling is predominantly parallel to the film[16] and should be greater in the region of large bubbles. Since the elastic and inelastic mean free paths are both ≈ 1000 Å in Al, the single loss spectrum of large bubbles should be comparatively enhanced because of less elastic scattering out of our narrow spectrometer aperture and fewer bulk plasmon losses.

EELS spectra at low energies for the 1.45-at.% specimen and a nonbombarded Al film are shown in Fig. 3. The features at 1.5, 6.75, and 15 eV are assigned to an Al band transition, the Al-Al_2O_3 surface plasmon, and the Al bulk plasmon, respectively. The remaining features, including the shoulders at 12 and 9.5 eV and the peak at 4 eV, can be associated with cavity plasmon losses, first predicted by Natta.[17] In the only previous observation of cavity modes, Henoc and Henry imaged He microbubbles in Al and obtained a low-resolution EELS spectrum with TEM in the electron-loss mode.[18] While the 12-eV shoulder in our high-resolution data can be identified as the dipole cavity mode, the interpretation of the two remaining features is less clear.[19]

We acknowledge helpful discussions with D. Ederer, B. Madden, G. Debras, A. Ronveaux, J. Ashley, G. Deconninck, C. Kunz, D. Eastman, and M. Kaminsky, and the assistance of the staff at LARN and SURF. This research has been supported, in part, by NATO Grant No. 1970 and the Belgian Ministry of Science Policy. One of us (S. D.) acknowledges the award of a fellowship from the Royal Society's European Science Exchange Programs.

[1]J. E. Inglesfield and J. B. Pendry, Philos. Mag. 34, 205 (1976).

[2]J. R. Cost and K. Y. Chen, J. Nucl. Mater. 67, 256 (1977).

[3]S. K. Das and M. Kaminsky, Adv. Chem. Sci. 158, 112 (1976); J. H. Evans, J. Nucl. Mater. 76-77, 396 (1978).

[4]W. Bauer, K. L. Wilson, C. L. Bisson, L. G. Haggmark, and R. J. Goldston, J. Nucl. Mater. 76-77, 396 (1978).

[5]K. Ohtaka and A. A. Lucas, Phys. Rev. B 18, 4643 (1978).

[6]S. E. Donnelly, J. C. Rife, J. M. Gilles, and A. A. Lucas, J. Nucl. Mater. 93-94, 767 (1980).

[7]J. Rife and J. Osantowski, Nucl. Instrum. Methods 172, 197 (1980).

[8]C. M. Surko, G. J. Dick, F. Reif, and W. C. Walker, Phys. Rev. Lett. 23, 842 (1969).

[9]J. C. Browne, Phys. Rev. 138, A9 (1965).

[10]S. L. Guberman and W. A. Goddard III, Phys. Rev. A 12, 1203 (1975).

[11]J. Jortner, N. R. Kestner, S. A. Rice, and M. H. Cohen, J. Chem. Phys. 43, 2614 (1965).

[12]E. C. Svensson, V. F. Sears, A. D. B. Woods, and P. Martel, Phys. Rev. B 21, 3638 (1980).

[13]J. O. Hirschfelder, C. F. Curtiss, and R. B. Bird, *Molecular Theory of Gases and Liquids* (Wiley, New York, 1954).

[14]D. Vidal and M. Lallemand, in *Physical Properties and Material Synthesis*, High Pressure Science and Technology, Vol. I, edited by K. D. Timmerhaus and M. S. Barber (Plenum, New York, 1979), p. 408.

[15]W. C. Martin, J. Res. Nat. Bur. Stand. 64, 19 (1960); H. Boersch, J. Geiger, and B. Schroder, Abh. Dtsch. Akad. Wiss. Berlin, Kl. Math. Phys. Tech., No. 1-15 (1976).

[16]S. E. Donnelly, G. Debras, J. M. Gilles, and A. Lucas, Rad. Eff. Lett. 50, 57 (1980).

[17]M. Natta, Solid State Commun. 7, 823 (1969).

[18]P. Henoc and L. Henry, J. Phys. (Paris), Colloq. 31, C1-55 (1970).

[19]Higher-order cavity mode losses should be much weaker. See J. C. Ashley and T. L. Ferrell, Phys. Rev. B 14, 3277 (1976).

Hot-Carrier Thermalization in Amorphous Silicon

Z. Vardeny and J. Tauc
Division of Engineering and Department of Physics, Brown University, Providence, Rhode Island 02912
(Received 29 December 1980)

Thermalization of photoinduced carriers in *a*-Si and *a*-Si:H was studied with use of subpicosecond-pump and probe techniques with parallel and perpendicular polarizations. The underlying process was identified as hot-carrier absorption whose cross section increases with the carrier excess energy. The energy dissipation rate in *a*-Si is $\simeq 0.5$ eV/ps ($\simeq \hbar\nu^2_{\text{phonon}}$) and is less than 0.1 eV/ps in *a*-Si:H; Fröhlich interaction with polar phonons can explain this smaller rate. A photoinduced dichroism associated with polarization memory was observed.

PACS numbers: 72.80.Ng, 72.20.Dp

We report the first observation of hot-carrier thermalization in amorphous semiconductors obtained from time-resolved studies of photoinduced absorption (PA) in the subpicosecond time domain. We could identify the underlying process as phonon-assisted hot-carrier absorption whose strength increases with increasing carrier excess energy ΔE. We found that the energy dissipation rate in *a*-Si is significantly higher than in *a*-Si:H and show that the difference can be understood if the energy dissipation in *a*-Si:H occurs via polar phonons while in *a*-Si all phonons are involved.

We used the pump and probe technique with a cavity-dumped passively mode-locked dye laser[1,2] producing linearly polarized light pulses at $\hbar\omega_p = 2$ eV with a single-side exponential shape and $t_p = 0.6$–0.8 ps duration, 1–2 nJ energy, and repetition rate of 10^6 s^{-1}. The probe beam passed through a polarization rotator and its polarization

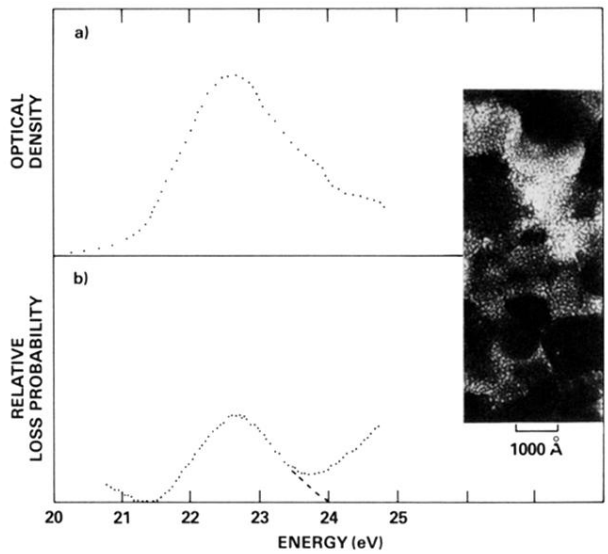

FIG. 1. 1.45 at.% He in Al. (a) Relative absorption spectrum (peak optical density is $\simeq 0.8$). (b) Electron-energy-loss spectrum (dashed line above 23 eV shows loss with multiple scattering removed). Inset: transmission electron micrograph.

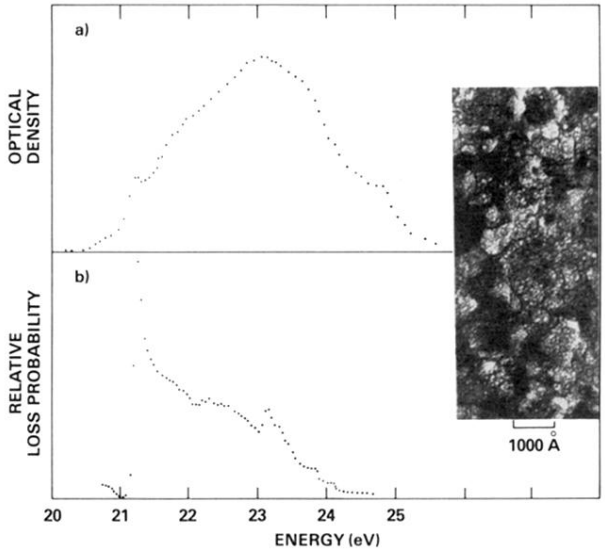

FIG. 2. 3.1 at.% He in Al. (a) Relative absorption spectrum (peak optical density is $\simeq 1.1$). (b) Electron-energy-loss spectrum. Inset: transmission electron micrograph.